



HAL
open science

Holes and cracks in rigid foam films

Pauline C. Petit, Marie Le Merrer, Anne-Laure Bianco

► **To cite this version:**

Pauline C. Petit, Marie Le Merrer, Anne-Laure Bianco. Holes and cracks in rigid foam films. *Journal of Fluid Mechanics*, 2015, 774, 10.1017/jfm.2015.278 . hal-01133820v2

HAL Id: hal-01133820

<https://hal.science/hal-01133820v2>

Submitted on 31 Mar 2015

HAL is a multi-disciplinary open access archive for the deposit and dissemination of scientific research documents, whether they are published or not. The documents may come from teaching and research institutions in France or abroad, or from public or private research centers.

L'archive ouverte pluridisciplinaire **HAL**, est destinée au dépôt et à la diffusion de documents scientifiques de niveau recherche, publiés ou non, émanant des établissements d'enseignement et de recherche français ou étrangers, des laboratoires publics ou privés.

Holes and cracks in rigid foam films

P. C. Petit ¹, M. Le Merrer ¹ and A.-L. Biance ^{1†},

¹Institut Lumière Matière, Université de Lyon, UMR5306 Université Lyon 1-CNRS, 69622
Villeurbanne, France

(Received xx; revised xx; accepted xx)

The classical problem of foam film rupture dynamics has been investigated when surfaces exhibit very high rigidity due to the presence of specific surfactants. Two new features are reported. First a strong deviation to the well-known Taylor-Culick law is observed. Then, crack-like patterns can be visualized in the film; these patterns are shown to appear at a well defined deformation. The key role of surface active material on these features is quantitatively investigated, pointing the importance of surface elasticity to describe these fast dynamical processes, and thus providing an alternative tool to characterize surface elasticity in conditions extremely far from equilibrium. The origin of the cracks and their consequences on film rupturing dynamics are also discussed.

1. Introduction

Despite its apparent useless character and simplicity, the dynamics of bursting of soap bubbles have fascinated scientists for more than a century. Lucien Bull (1904) made the first images of soap bubble bursts. The first theoretical analysis dates back to Dupré and then to Taylor (1959) and Culick (1960) where they considered the presence of a rim at the edge of a hole created in the liquid film, collecting the liquid during its movement. The constant hole opening velocity V_c results from a balance between the rim inertia and surface tension in the film, and is given by $V_c = \sqrt{2\gamma_{\text{eq}}/(\rho h_0)}$, with γ_{eq} the equilibrium surface tension, ρ the liquid density and h_0 the film thickness. These results are in good agreement with stationary experiments performed on liquid sheet (Taylor 1959) and has been extensively investigated by McEntee & Mysels (1969) in the case of soap films thicker than 50 nm. More recently, satellite formation during edge retraction (Lhuissier & Villermaux 2009*b*) and bubble entrapment (Bird *et al.* 2010) have been investigated as these behaviors are crucial in many applications. Destabilization of liquid sheets or bubbles indeed arise in many practical situations ranging from the building material industry, when glass sheets are molded, to foam engineering, food processing, biological membrane and environmental science (Bird *et al.* 2010). In these applications, liquids can be viscous or contain surface active materials. In the latter, surface tension becomes a dynamical quantity, which depends on the local surface concentration of surfactants, and thus on the elongation of the surface; this is characterized by the surface elasticity defined as the derivative of surface tension with respect to relative changes in surface area. The effect of surface elasticity has been observed through the development of an aureole surrounding the opening hole and expanding with time (Florence & Frens 1972; Liang *et al.* 1996; Lhuissier & Villermaux 2009*a*). However, except in the case of very viscous liquid, the opening dynamics always obey Taylor-Culick law, although some deviations have been reported by Mysels (McEntee & Mysels 1969; Florence & Mysels 1974), but hardly commented. In this work, we investigate the dynamics of bursting of circular foam films generated from surfactant solutions inducing large surface elasticities and we report

† Email address for correspondence: anne-laure.biance@univ-lyon1.fr

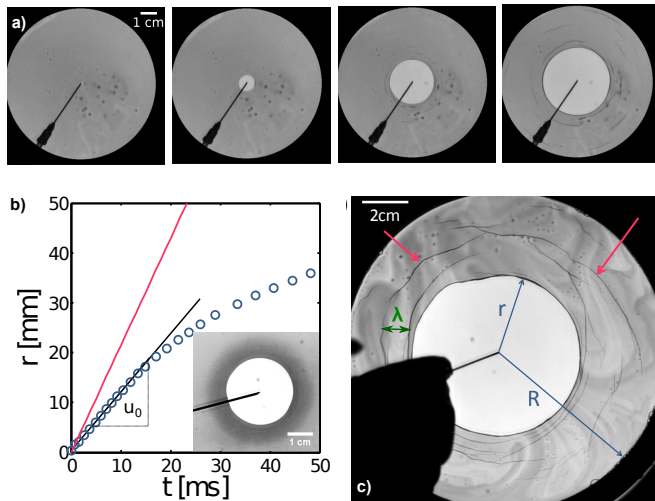


FIGURE 1. (a) Image sequence of a foam film rupture ($h_0=10 \mu\text{m}$, solution E – table 1). The timelapse between images is 8 ms. (b) Radius r of the hole *vs* time t ($h_0=10 \mu\text{m}$, solution E). The red (light) line represents the prediction of Taylor-Culick, while the black line shows the initial opening at constant velocity u_0 . Inset: Picture of a ruptured foam film (solution C) which highlights aureole formation. (c) Picture of a foam film (solution E) 37 ms after its breaking. The arrows highlight crack-like patterns, which appear during the hole opening.

for the first time systematic deviations to Taylor-Culick law. A careful analysis allows us to estimate surface elasticity at both large compression and compression rate in good agreement with reported data in the literature. Moreover, unexpected effects of frame size are observed through the appearance of new patterns, reminiscent of fractures or wrinkles in the film.

2. Experimental set-up

The experimental set-up consists in a circular metallic frame of radius $R = 1.5 - 11 \text{ cm}$ pulled out from a surfactant solution at different velocities to generate films with various thicknesses. The film absolute thickness is determined through an absorption technique measurement (Lastakowski *et al.* 2014; Petit *et al.* 2015) and we denote h_0 the initial average thickness of the film. Film rupture is initiated by approaching a heated needle and is recorded via a high-speed camera (10000 Hz, Photron SA-4). An image sequence is reported in figure 1a, where we measure the radius r of the expanding hole versus time, as shown in figure 1b. Surfactant solutions are produced in a 10%-90% glycerol-water mixture in which a dye (Brilliant Black BN 60%, Sigma, 5g/L) is added. They contain 3.3 g.L^{-1} of sodium lauryl-dioxyethylene sulfate (SLES, Stepan), 1.7 g.L^{-1} of cocoamidopropyl betaine (CAPB, Goldschmidt) and myristic acid (MAc, Fluka) in the concentrations C described in table 1. The surface elasticities of similar solutions are well characterized in the literature (Mitrinova *et al.* 2013a) and span over two orders of magnitude when the concentration C of MAc is varied as reported in table 1. Such elastic moduli are attributed to the surface properties of the adsorbed layer of MAc, whose surface concentration is expected to increase with C up to the saturation of the surface (Golemanov *et al.* 2008). At the same time, micelles of the two co-surfactants (SLES and CAPB) help to solubilize the poorly soluble fatty acid.

Solution	A	B	C	D	E	F
C [mM]	-	0.055	0.11	0.22	0.88	2.2
γ_{eq} [mN/m]	29	29	27	26	23	22
E_{od} [mN/m]	4	50	90	200	400	400
$E_0(u_0)$ [mN/m]	60	200	2000	5000	2.10^4	4.10^4
$E_0(\text{cracks})$ [mN/m]	-	-	90	200	300	300

TABLE 1. Properties of the surfactant solutions used in the experiments: MAC concentration C , equilibrium surface tension γ_{eq} and surface elasticities. Data from Mitrinova *et al.* (2013a) for similar solutions (without glycerol and dye) are reported for γ_{eq} and the elastic modulus E_{od} measured with the oscillating drop method for small deformation (0.2–4 %) at frequency 0.2 Hz. $E_0(u_0)$ corresponds to the elasticity deduced from the initial hole velocity using equation (4.1). $E_0(\text{cracks})$ corresponds to the elasticity deduced from cracking radius using equation (4.2).

3. Results

Some remarkable features can be underlined. At first, the opening velocity is constant as expected but smaller than predicted by Taylor-Culick law (figure 1b). Moreover, an aureole already described in the past (Florence & Frens 1972; Liang *et al.* 1996; Lhuissier & Villermaux 2009a) is observed through spatial variations of transmitted light, especially for the less rigid interfaces (inset of figure 1b). Then, some dark patterns are observed (see arrows in figure 1c), which we denote *cracks* in the following. This apparition coincides with a decrease of the opening velocity (figure 1b), the presence of these cracks modifying the bursting dynamics.

The initial opening velocity u_0 is represented in figure 2a as a function of the initial film thickness h_0 for various solutions. Without MAC (solution A of table 1), the velocity follows Taylor-Culick law (\circ), which is consistent with interfaces of low elasticity. However, in the presence of MAC, the initial velocity is lower than in the previous case. For each MAC concentration, the initial velocity varies with $1/\sqrt{h_0} \propto V_c$. For each solution and different thicknesses, we thus extract the initial opening velocity normalized by Culick velocity. This quantity decreases when the MAC concentration increases (figure 2b), that is, for larger surface elastic moduli (Mitrinova *et al.* 2013a).

During the film opening, orthoradial cracks (perpendicular to the direction of opening) appear in the film (figures 1a and 1c), at a well defined radius of the hole r_p . Some specific irregular fold-like patterns and filaments have been previously reported by McEntee & Mysels (1969), although not directly comparable to our observations. For a given solution, figure 3a shows that the ratio r_p/R is independent of the frame radius (for $R = 1.5 - 11$ cm) and almost independent of the film thickness (for $h_0 = 2 - 20$ μm). The cracks thus appear for a well-defined critical compression of the interface. Figure 3b shows that this critical compression decreases with MAC concentration and the surface modulus.

4. Discussion

These two observations concerning the initial opening velocity and the onset compression for cracks can be rationalized following the framework initially proposed by Frankel & Mysels (1969) for the theoretical description of aureoles. They considered that surfactants are insoluble, which is reasonable at the timescale considered here: the duration of the opening R/u_0 , typically 30 ms, is smaller than surfactant desorption time

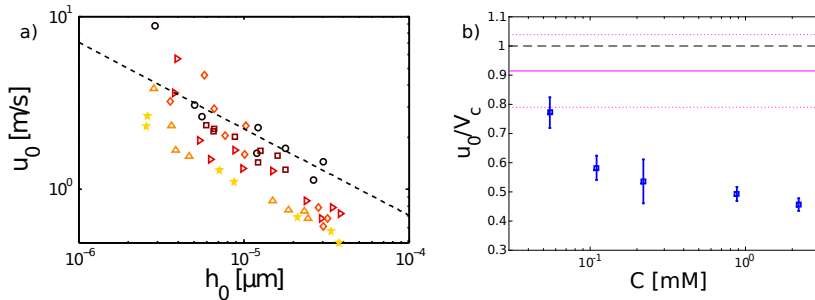


FIGURE 2. (a) Initial opening velocity u_0 of the hole as a function of the film thickness h_0 for $R = 3$ cm. The MAC concentration C decreases from dark to light points: solutions A (o), B (\square), C (\triangleright), D (\diamond), E(\triangle) and F (\star). (b) initial opening velocity normalized by Culick velocity u_0/V_c as a function of C (error bars: 95 % confidence intervals). The magenta solid line shows the value measured for $C = 0$, with error bars shown by the dotted lines. The values u_0/V_c are extracted by performing least square percentage fit for each solution, with weights taking into account the $1 \mu\text{m}$ error on thickness measurements. In both figures, the black dashed lines represent Taylor-Culick law.

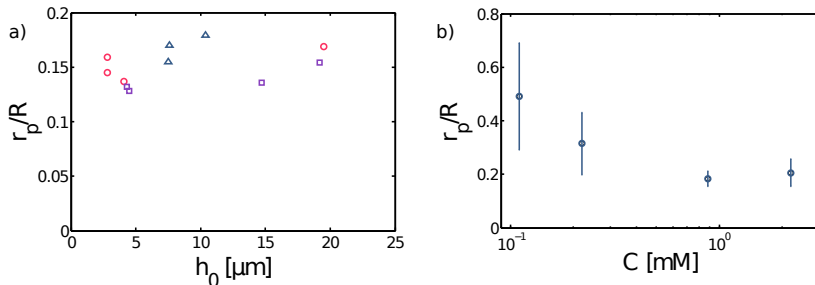


FIGURE 3. (a) Critical compression of the interface for crack formation r_P/R as a function of the initial thickness h_0 for solution E and different frame radii $R = 1.5$ cm (o), $R = 3$ cm (\square) et $R = 11$ cm (\triangle). (b) r_P/R averaged for thicknesses $h_0 = 2 - 35 \mu\text{m}$ and $R = 3$ cm, as a function of MAC concentration C .

τ . Indeed, although these processes are likely to be dominated by surfactant exchange with micelles in our systems (Golemanov *et al.* 2008), a lower bound for τ is provided by the diffusion time across the film thickness $h_0^2/D \approx 40 \text{ ms} - 2 \text{ s}$ (for $h_0 = 2 - 40 \mu\text{m}$ and $D = 10^{-10} \text{ m}^2/\text{s}$). Adsorption times longer than 30 ms for myristic acid in these systems have also been reported (Mitrinova *et al.* 2013b). A compressive shock thus propagates at the surface of the film. The liquid is collected in an extended rim — an *aureole* — visible in figure 1b (inset) and whose shape depends on surface tension, film thickness and surface elasticity.

Viscous effects have also been neglected. Indeed, as no shear takes place within the film thickness, the characteristic Reynolds number and *surface* Reynolds numbers read $Re = u_0 R/\nu \gg 1$ and $Re_s = \rho u_0 R h_0/\kappa$, respectively, with ν the kinematic bulk viscosity and κ the intrinsic surface viscosity. Surface viscous dissipation can *a priori* not be neglected if values of κ measured at 0.2 Hz are considered (Costa 2012; Golemanov *et al.* 2008). However, surface viscosity is expected to collapse at large frequencies, as shown in experiments and modeling (Lucassen & Van Den Tempel 1972). Eventually, the observation of a constant initial velocity varying with $1/\sqrt{h_0} \propto V_c$ (figures 1b and 2) is a key indication that inertia (and not viscous effects) is dominant in this problem.

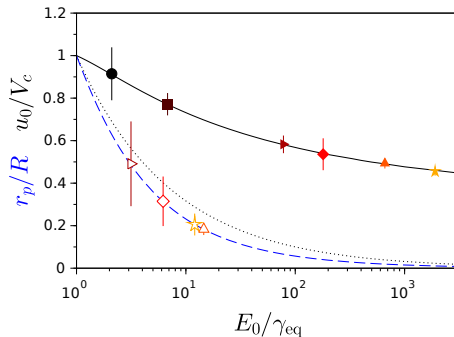


FIGURE 4. Solid black line: numerical prediction for the normalized hole velocity $u_0/V_c = f(E_0/\gamma_{\text{eq}})$ for radial bursting (equation (4.1) and A). The dashed line corresponds to $u_0/V_c = \sqrt{\gamma_{\text{eq}}/E_0}$ expected for unidimensional bursting (Frankel & Mysels 1969). Blue dashed line: prediction for the critical radius at which cracks appear $r_p/R = \sqrt{\gamma_{\text{eq}}/E_0} f(E_0/\gamma_{\text{eq}})$ (equation (4.2)). The solid (resp. empty) symbols correspond to the experimental data from figure 2 (resp. figure 3), from which we determine the elastic moduli $E_0(u_0)$ (resp. $E_0(\text{cracks})$). Same symbols and colors as in figure 2a.

4.1. Deviation to Taylor-Culick law

The dynamics of the rim is then controlled by the balance between inertia and surface tension spatial gradient. We assume here that surface elasticity is constant up to a certain compression. In this particular case, the velocity of the aureole front (delimiting the frontier with the zone of undisturbed film whose thickness is still $h = h_0$) simply reads $u_f = \sqrt{2E_0/(\rho h_0)} = V_c \sqrt{E_0/\gamma_{\text{eq}}}$, which can be seen as a two dimensional analogous of sound (compression) velocity. The opening hole velocity can also be determined by solving the self-similar profile of the aureole and applying mass conservation. No analytical solution is provided in the considered radial geometry but numerical resolution shows that

$$u_0 = V_c f(E_0/\gamma_{\text{eq}}) \quad (4.1)$$

with f a decreasing function determined numerically (see appendix A) and reported in figure 4. It is thus still proportional to Taylor-Culick velocity V_c and decreases with the interfacial elasticity E_0 , which is consistent with experimental observations of figure 2. From these data and equation (4.1), an interfacial elasticity $E_0(u_0)$ can be deduced (figure 4), which is reported in table 1 as a function of the MAc concentration. These data are compared to measurements of surface moduli E_{od} from the oscillating drop method performed by Mitrinova *et al.* (2013a). It shows the same qualitative variation with C despite a discrepancy on the absolute values obtained. However, the shrinkage amplitude and the compression timescales differ by several orders of magnitude, and the surfactant monolayer at the interface is expected to be highly non-Newtonian (Costa 2012; Lucassen & Van Den Tempel 1972).

4.2. Crack appearance

Besides, snapshot inspection shows that cracks appear when the compressive surface wave (i.e. the aureole front) reaches the metallic frame of the film. Cracks are thus expected for:

$$\frac{r_p}{R} = \frac{u_0}{u_f} = \sqrt{\frac{\gamma_{\text{eq}}}{E_0}} f\left(\frac{E_0}{\gamma_{\text{eq}}}\right) \quad (4.2)$$

This prediction, represented in figure 4, is indeed in good agreement with our observations: The hole radius when cracks appear r_p increases with the frame radius R and decreases with surface elasticity probed through MAc concentration variations, as shown in figure 3. Eventually, this critical compression does not depend on film thickness h_0 , showing that elasticity is not affected by confinement in the experimental configuration tested.

The surface elasticity $E_0(\text{cracks})$ can therefore be deduced from the critical radius for crack apparition r_p (figure 4), and reported for the different MAc concentration in table 1. In this case, a very good agreement is obtained with the measured value of the surface modulus (Mitrinova *et al.* 2013a), which confirms that the cracks arise from a compression of the aureole when its front reaches the frame.

Note that the values of surface elasticity deduced from our two methods may differ. This is however expected due to our strong hypothesis of constant elasticity. Indeed, while the aureole front velocity only depends on the surface elasticity at very low compression rate (at the edge of the undisturbed film), the hole opening velocity modeling takes into account the elasticity through large interface compression. For large deformation, it is expected that the constant elasticity model fails: at large compression, the myristic acid surface concentration increases, which should result in larger elasticity as can be inferred from the moduli dependency upon C (Mitrinova *et al.* 2013a). The effective modulus $E_0(u_0)$ should then deviate more from measurements at small deformations performed by the oscillating bubble technique (Mitrinova *et al.* 2013a).

In addition, the effect of elasticity has indirect consequences of some features of foam film rupture. For example, no flapping nor transverse destabilization of the rim was observed for our rigid soap films, in contrast to observations on low elasticity films and theoretical predictions (Lhuissier & Villermaux 2009b); however, the reduced rim velocity could prevent the flapping instability to develop and subsequent film atomization (Lhuissier & Villermaux 2009b).

4.3. Crack-like patterns

Let us now discuss the observed crack-like patterns. During the fast deformation of the surface, the surfactants behave as an insoluble monolayer, comparable to a lipid monolayer experiencing a compression in a Langmuir trough (Lee 2008). In this case, above a critical compression, such a monolayer can behave differently depending on its structure. If it is liquid-like, it ejects the molecules in the bulk in the form of vesicles or bilayers. If it is solid-like, it can bend as an elastic sheet or fracture as a fragile material.

Although our experiment does not provide a microscopic characterization of this transient surface structure, the crack pattern can be macroscopically characterized. In particular, even though the cracks are irregularly distributed, a number of cracks per radial segment can be counted; the deduced characteristic length between two cracks denoted λ (figure 1c) is reported in figure 5 as a function of MAc concentration C (a) and film thickness h_0 (b).

The increase of λ with C is expected whatever the mechanism proposed. On the one hand, for higher bulk concentration, solubilization of interfacial surfactants is more difficult, hence a reduced number of vesicles or bilayers are to be expelled. On the other hand, a more concentrated solid-like layer will also exhibit a higher bending modulus and wavelength of elastic ripples are expected to increase with this modulus (Cerdea & Mahadevan 2003). The decrease of the characteristic length with the film thickness h_0 is more unexpected. For the solid-like behavior, a thinner elastic sheet will bend more easily than a thicker one, thus exhibiting smaller ripple wavelength when buckled (Landau & Lifshitz 1975), in contrast with our observations. If cracks correspond to monolayer

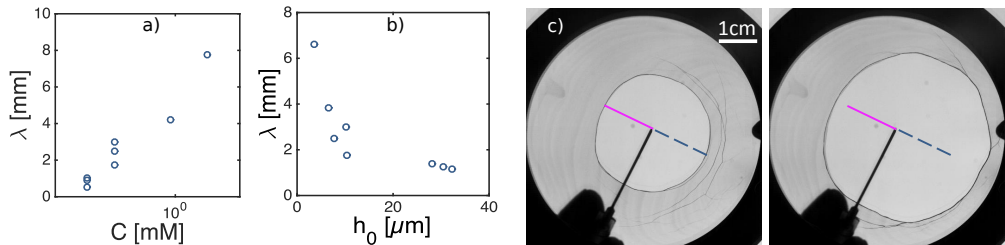


FIGURE 5. (a) Characteristic length λ between two cracks as a function of MAc concentration C for $h_0 = 11 \pm 3 \mu\text{m}$. (b) λ as a function of the film thickness h_0 for solution D. (c) Bursting of a soap film of thickness $h_0 = 3 \mu\text{m}$ (solution E). The timelapse between the two images is 9 ms, and the two lines highlight the velocity inhomogeneities.

collapse by vesicles formation, it should not be affected by the film thickness. However, when modifying the thickness of the film, we also vary the velocity of compression or shrinkage rate. This parameter induces dynamical structural change in the surfactant monolayers (as it does in bulk crystallization processes for example (Cabane & Hénon 2003)).

Finally, a complete understanding of the origin of these crack-like patterns would require some local high speed imaging structural analysis, which are beyond the scope of the present paper.

The presence of these irregular cracks have direct consequences on hole opening dynamics. Indeed, when the aureole reaches the metallic frame, the hole opening slows down (and even stops for the thinner rigid films) and then irregularly accelerates in the region where the cracks appears. This feature is reported in figure 5c. Moreover, a velocity discontinuity in the liquid is observed, the outer region being at rest whereas the inner region is deformed.

5. Conclusion

To conclude, we have shown that modifying the chemistry of surfactant solutions can have strong influences on macroscopic dynamical processes, as observed in various situations in foams and foam films (Couder *et al.* 1989; Durand & Stone 2006; Seiwert *et al.* 2013; Petit *et al.* 2015; Lorenceau *et al.* 2009). However, we have investigated here this effect under large deformations and in a fast dynamical process, *i.e.* at large Reynolds numbers, where the effects of molecular scales and surfactants are expected to be negligible.

The initial constant velocity opening dynamics is well described taking into account the surface elasticity of the interfaces and was shown to be reduced at high surface modulus. This may be responsible for the inhibition of rim fragmentation and droplet ejection usually reported in liquid film ruptures (Lhuissier & Villermaux 2009b). Further studies should determine the role of the ejected droplets in rupture propagation in macroscopic foams; the stability of these systems is indeed known to depend dramatically on the surface elastic properties (Rio & Biance 2014). However, finite size effects becomes soon crucial: when the elastic compression surface wave reaches the border of the frame, crack-like patterns, where velocity discontinuity are observed, appear in the foam film. Determining the origin of cracks, their microscopic structure, their location and number, and how they control film opening dynamics remain a challenge to tackle.

The authors thank Gilles Simon for his help in setting up the experiment.

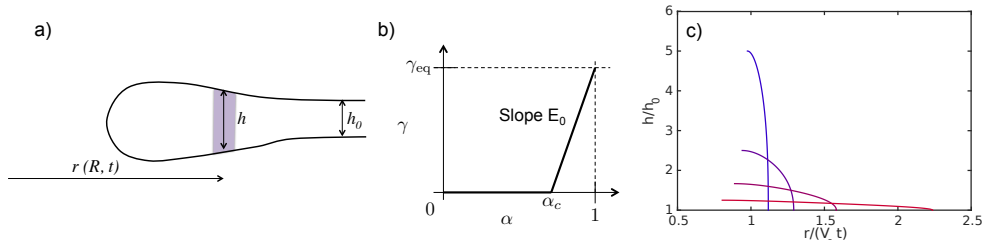


FIGURE 6. (a) Profile of the film and notations. (b) Variations of surface tension γ versus shrinkage α in the simplified constant elasticity modeling. (c) h/h_0 as a function of $r/(V_c t) = \sqrt{2w/V_c^2}$ for radial bursting and different values of α_C (0.2, 0.4, 0.6, 0.8 from top to bottom at the origin).

Appendix A

Equations for radial bursting

We describe the radial bursting dynamics of a foam film of initial uniform thickness h_0 and include the effect of dynamic surface tension as first proposed by Frankel & Mysels (1969): the surface tension γ is assumed to depend only on the shrinkage of the surface α which by mass conservation is related to film thickness $\alpha = h_0/h$. We denote the surface elasticity $E(\alpha) = \frac{d\gamma}{d\alpha}$. As viscous terms are negligible, the capillary forces are balanced by the fluid inertia. Variations of fluid velocity across the film are also neglected and equations are averaged over h . These equations can be explicitly solved in the unidimensional case (Frankel & Mysels 1969). However, in the case of radial bursting, a numerical resolution is necessary.

We consider a material element that has initially the position R (*i.e.* that has Lagrangian variables (R, t)). At instant t , its position is $r(R, t)$ and its thickness $h(R, t)$ (figure 6a). The fluid velocity is $u = \partial r / \partial t$ and the shrinkage is defined as $\alpha = h/h_0 \partial r^2 / \partial R^2 = (r/R) \partial r / \partial R$. The momentum balance on the fluid element yields

$$\rho h \frac{\partial u}{\partial t} = 2r \frac{\partial \gamma}{\partial r}$$

which can be rewritten

$$\frac{\partial u}{\partial t} = \frac{2E(\alpha)}{\rho h_0} \frac{r}{R} \frac{\partial \alpha}{\partial R} = U_\alpha^2 \frac{r}{R} \frac{\partial \alpha}{\partial R} \quad (\text{A } 1)$$

in which we have defined the characteristic velocity

$$U_\alpha = \sqrt{\frac{2E(\alpha)}{\rho h_0}}.$$

Following the analysis of Frankel & Mysels (1969), we are looking for self-similar solutions in the form $r/t = f(R/t)$. We define the variables $W = R^2/(2t^2)$ and $w = r^2/(2t^2)$ (w and W have the dimensions of square velocities) and we expect $w = w(W)$. The relative shrinkage is also set by $\alpha = dw/dW$. Starting from equation (A 1), we find

$$\frac{W}{w} \left[1 - \frac{W}{w} \frac{dw}{dW} \right] \frac{dw}{dW} = \left[U_{\alpha=dw/dW}^2 - \frac{2W^2}{w} \right] \frac{d^2 w}{dW^2} \quad (\text{A } 2)$$

A first information on the film dynamics can be inferred from this equation: Far from the hole, *i.e.* for large W , the film should remain undisturbed, which corresponds to $w = W$ and $dw/dW = 1$. This condition combined with equation (A 2) yields

$\left[U_{\alpha=1}^2 - \frac{2W^2}{w} \right] \frac{d^2w}{dW^2} = 0$, which implies that the matching with the disturbed film can only be done at $W = W_0 = U_{\alpha=1}^2/2$. The velocity of the front of the *aureole*, or extended rim corresponding to the disturbed film, is thus given by $u_f = U_{\alpha=1}$ (Frankel & Mysels 1969).

Finally, the complete aureole profile and hole receding velocity will depend on the form of the elasticity versus shrinkage.

Numerical resolution for a constant elasticity model

We consider at first order a model of constant elasticity E_0 , as described in figure 6b. We introduce here α_c , which corresponds to the maximum shrinkage the film can endorse. For $\alpha > \alpha_c$, the surface elasticity is constant and reads

$$\frac{d\gamma}{d\alpha} = E_0 = \gamma_{\text{eq}} \frac{1}{1 - \alpha_c}$$

and then

$$U_\alpha = U_0 = \sqrt{\frac{2E_0}{\rho h_0}} = \sqrt{\frac{E_0}{\gamma_{\text{eq}}}} V_c$$

where $V_c = \sqrt{2\gamma_{\text{eq}}/(\rho h_0)}$ is Culick velocity.

When $\alpha > \alpha_c$, equation (A 2) can be written as

$$\frac{W}{w} \left[1 - \frac{W}{w} \frac{dw}{dW} \right] \frac{dw}{dW} = \left[U_0^2 - \frac{2W^2}{w} \right] \frac{d^2w}{dW^2} \quad (\text{A } 3)$$

In non-dimensionalized form (stating $\tilde{W} = 2W/V_c^2$ and $\tilde{w} = 2w/V_c^2$), this equation reduces to

$$\frac{\tilde{W}}{\tilde{w}} \left[1 - \frac{\tilde{W}}{\tilde{w}} \frac{d\tilde{w}}{d\tilde{W}} \right] \frac{d\tilde{w}}{d\tilde{W}} = \left[\frac{1}{1 - \alpha_c} - \frac{2\tilde{W}^2}{\tilde{w}} \right] \frac{d^2\tilde{w}}{d\tilde{W}^2} \quad (\text{A } 4)$$

with the two following boundary conditions. In $\tilde{W} = 0$, at the hole, we have the maximum shrinkage (minimum value of α_c): $\frac{d\tilde{w}}{d\tilde{W}}(\tilde{W} = 0) = \alpha_c$. In $\tilde{W} = \tilde{W}_0 = \frac{1}{2(1-\alpha_c)}$, at the aureole front, the solution should match the undisturbed film solution $\tilde{w}(\tilde{W}_0) = \tilde{W}_0$.

This equation is solved numerically with a shooting method. From the function $w(W)$, we can deduce the thickness profile, using the relation $h/h_0 = 1/(dw/dW)$ for different elasticities (figure 6c). As the elasticity increases (i.e. as α_c becomes closer to 1), we find that the aureole is thinner and wider, while for $E_0 = \gamma_{\text{eq}}$ (corresponding to $\alpha_c = 0$), one recovers a punctual rim receding at Taylor-Culick velocity V_c .

We can also estimate the initial hole velocity $u_0 = \sqrt{2w(W=0)}$, which is shown in figure 4 as a function of the ratio E_0/γ_{eq} . We also observe that the results obtained deviate from those obtained for unidimensional bursting (Frankel & Mysels 1969), especially for large elasticities, emphasizing the crucial role of radial geometry.

REFERENCES

- BIRD, JAMES C., DE RUITER, RIELLE, COURBIN, LAURENT & STONE, HOWARD A. 2010 Daughter bubble cascades produced by folding of ruptured thin films. *Nature* **465** (7299), 759–762.
- CABANE, B. & HÉNON, S. 2003 *Liquides– Solutions, dispersions, gels*. Belin.
- CERDA, E. & MAHADEVAN, L. 2003 Geometry and physics of wrinkling. *Physical Review Letters* **90** (7), 074302.

- COSTA, SÉVERINE 2012 Rhéologie multi-échelle des mousses liquides. PhD thesis, Université Paris-Est Marne La Vallée.
- COUDER, Y., CHOMAZ, J. M. & RABAUD, M. 1989 On the hydrodynamics of soap films. *Phys. D* **37** (1-3), 384–405.
- CULICK, F. E. C. 1960 Comments on a ruptured soap film. *Journal of Applied Physics* **31** (6), 1128–1129.
- DURAND, M. & STONE, H. A. 2006 Relaxation time of the topological T1 process in a two-dimensional foam. *Physical Review Letters* **97**, 226101.
- FLORENCE, A. T. & FRENS, G. 1972 Aureole profile in bursting soap films - Surface-tension and surface relaxation in rapidly compressed monolayers. *Journal of Physical Chemistry* **76** (21), 3024–3029.
- FLORENCE, ALEXANDER T. & MYSELS, KAROL J. 1974 Bursting of soap films. VI. effect of surfactant purity. *The Journal of Physical Chemistry* **78** (3), 234–235.
- FRANKEL, S. & MYSELS, K. J. 1969 Bursting of soap films .2. Theoretical considerations. *Journal of Physical Chemistry* **73** (9), 3028–3038.
- GOLEMANOV, K., DENKOV, N. D., TCHOLAKOVA, S., VETHAMUTHU, M. & LIPS, A. 2008 Surfactant mixtures for control of bubble surface mobility in foam studies. *Langmuir* **24** (18), 9956–9961.
- LANDAU, L. D. & LIFSHITZ, E. M. 1975 *Elasticity Theory*. Oxford: Pergamon Press.
- LASTAKOWSKI, H., BOYER, F., BIANCE, A. L., PIRAT, C. & YBERT, C. 2014 Bridging local to global dynamics of drop impact onto solid substrates. *Journal of Fluid Mechanics* **747**, 103–118.
- LEE, K. Y. C. 2008 Collapse mechanisms of Langmuir monolayers. *Annu. Rev. Phys. Chem.* **59**, 771–791.
- LHUISSIER, H. & VILLERMAUX, E. 2009a Destabilization of flapping sheets: The surprising analogue of soap films. *Comptes Rendus Mécanique* **337** (6-7), 469–480.
- LHUISSIER, H. & VILLERMAUX, E. 2009b Soap films burst like flapping flags. *Physical Review Letters* **103** (5), 054501.
- LIANG, N. Y., CHAN, C. K. & CHOI, H. J. 1996 Dynamics of the formation of an aureole in the bursting of soap films. *Physical Review E* **54** (4), R3117–R3120.
- LORENCEAU, E., LOUVET, N., ROUYER, F. & PITOIS, O. 2009 Permeability of aqueous foams. *Eur. Phys. J. E* **28**, 293–304.
- LUCASSEN, J. & VAN DEN TEMPEL, M. 1972 Dynamic measurements of dilational properties of a liquid interface. *Chemical Engineering Science* **27** (6), 1283 – 1291.
- MCENTEE, W. R. & MYSELS, K. J. 1969 Bursting of soap films .i. An experimental study. *Journal of Physical Chemistry* **73** (9), 3018–3028.
- MITRINOVA, Z., TCHOLAKOVA, S., GOLEMANOV, K., DENKOV, N., VETHAMUTHU, M. & ANANTHAPADMANABHAN, K. P. 2013a Surface and foam properties of SLES plus CAPB plus fatty acid mixtures: Effect of pH for C12-C16 acids. *Colloids and Surfaces A-physicochemical and Engineering Aspects* **438**, 186–198.
- MITRINOVA, Z., TCHOLAKOVA, S., POPOVA, Z., DENKOV, N., DASGUPTA, BIVASH R. & ANANTHAPADMANABHAN, K. P. 2013b Efficient control of the rheological and surface properties of surfactant solutions containing C8-C18 fatty acids as cosurfactants. *Langmuir* **29** (26), 8255–8265.
- PETIT, P., SEIWERT, J., CANTAT, I. & BIANCE, A.-L. 2015 On the generation of a foam film during a topological rearrangement. *Journal of Fluid Mechanics* **763**, 286–301.
- RIO, EMMANUELLE & BIANCE, ANNE-LAURE 2014 Thermodynamic and mechanical timescales involved in foam film rupture and liquid foam coalescence. *ChemPhysChem* **15** (17), 3692–3707.
- SEIWERT, J., MONLOUBOU, M., DOLLET, B. & CANTAT, I. 2013 Extension of a suspended soap film: A homogeneous dilatation followed by new film extraction. *Physical Review Letters* **111** (9), 094501.
- TAYLOR, G. 1959 The dynamics of thin sheets of fluid .3. Disintegration of fluid sheets. *Proceedings of the Royal Society of London Series A-Mathematical and Physical Sciences* **253** (1274), 313–321.